Exceptionally accelerated Fe(III)/Fe(II) redox couple by niobium carbide MXene: A green and long-lasting enhanced Fenton oxidation

Zixuan Zhang [a,b], Chenying Zhou [a,b], Yiming Sun [a,b], Peng Zhou [a,b,*], Yang Liu [a,b], Heng Zhang [a,b], Ye Du [a,b], Chuanshu He [a,b], Zhaokun Xiong [a,b], Bo Lai [a,b,*]

[a] State Key Laboratory of Hydraulics and Mountain River Engineering, College of Architecture & Environment, Sichuan University, Chengdu 610065, China
[b] Sino-German Centre for Water and Health Research, Sichuan University, Chengdu 610065, China

ABSTRACT

Fenton oxidation technology is a widely-used advanced oxidation technology. However, the generation of hydroxyl radicals is restrained by the sluggish recovery of Fe(II), thus affecting its long-lasting performance for water decontamination. Here, a novel niobium carbide (Nb_2C) MXene material was applied as a green co-catalyst. Nb_2C MXene can significantly promote Fenton reactions to produce hydroxyl radicals for degrading dimethyl phthalate (DMP) with high efficiency and high stability for long-term operation, which outperforms than various reported co-catalysts. Meanwhile, the Nb_2C/Fe(III)/H_2O_2 system is capable of non-selectively degrading a wide spectrum of refractory pollutants. Mechanism investigation reveals that Nb_2C MXene as an electron donor can straight reduce Fe(III), meanwhile mediate electron shuttle from Fe(II) to H_2O_2 to strongly expedite the generation of hydroxyl radicals. In addition, four main degradation routes of DMP were proposed. Therefore, this study offers an updated and valid strategy for the refractory organic pollutants elimination by coupling Nb_2C MXene and Fenton oxidation.

1. Introduction

Phthalate esters (PAEs) are a common plasticizer, often used in combination with polymer materials to enhance their flexibility, ruggedness and service life [1]. Due to their low molecular weight and physical bonding in the polymer, PAEs are gradually released into environment waters [2]. Recently, seeking for state-of-the-art strategies to degrade PAEs has become an important issue in environmental remediation resulting from their potential risks of organ damage, cancer, and endocrine system [3,4].

Fenton technology can produce reactive hydroxyl radicals (•OH) for oxidizing refractory organics with high reaction constants, simple operation, mild reaction conditions as well as low toxic by-products [5, 6]. In classical Fenton system (Eq. 1~9), the peroxide O-O bond of hydrogen peroxide (H_2O_2) is able to be effectively decomposed by Fe(II) to produce hydroxyl radicals (Eq. 1). Nevertheless, the intrinsic drawbacks of traditional Fenton technology strongly limit its practical application towards real industry wastewaters, especially the sluggish kinetic of Fe(II) regeneration (Eq. 2) caused low H_2O_2 utilization rate [7,

8], high Fe(II) dosage and amount iron sludge (e.g., iron (oxyhydr)oxides) [9,10]. For overcoming these shortcomings, many new tactics were tried to expedite Fe(III) reduction and H_2O_2 decomposition, reduce Fe(II) dosage, and alleviate iron sludge precipitation, such as inputs of co-catalysts or energy (e.g., electricity and ultraviolet light) [11–13]. Among these strategies, a variety of co-catalysts as chelating agents or electron sacrifices were recently coupled with Fenton/Fenton-like systems to oxidize organic contaminants by achieving rapid Fe(II)/Fe(III) redox couple. Dissolved co-catalysts include hydroxylamine, protocatechuic acid, and ascorbic acid, which were initially applied to boost Fenton oxidation with high removal efficiencies to target contaminants, however, hydroxyl radical quenching effects ($k_{(protocatechuic acid)}= 5.0 \times 10^9 M^{-1} s^{-1}$; $k_{(hydroxylamine)} = 1.83 \times 10^2 M^{-1} s^{-1}$; $k_{(ascorbic acid)}= 1.2 \times 10^{10} M^{-1} s^{-1}$) with co-catalysts derived secondary organic pollutions cause barriers for their practical application [14–16]. Subsequent literatures proposed that some heterogenous co-catalysts also be able to mightily expedite Fe(III) reduction to enhance Fenton oxidation, such as crystalline boron and metal sulfides [17–19]. For all that these heterogeneous co-catalysts significantly alleviate ROS quenching, the

decomposition of boron and metal sulfides also cannot avoid secondary pollution (e.g., boron leaching and metal leaching) [19,20]. Therefore, the achievement of sustainable Fenton oxidation requires the development of green and long-lasting heterogeneous co-catalysts.

$$Fe(II) + H_2O_2 \rightarrow \bullet OH + OH^- + Fe(III) \; 40–80 \; M^{-1} \; s^{-1} \quad (1)$$

$$Fe(III) + H_2O_2 \rightarrow HO_2^\bullet + H^+ + Fe(II) \; 9 \cdot 1 \times 10^{-7} \; M^{-1} \; s^{-1} \quad (2)$$

$$Fe(III) + HO_2^\bullet \rightarrow O_2 + H^+ + Fe(II) \quad (3)$$

$$Fe(II) + \bullet OH \rightarrow Fe(III) + OH^- \quad (4)$$

$$Fe(II) + HO_2^\bullet \rightarrow Fe(III) + HO_2^- \quad (5)$$

$$\bullet OH + \bullet OH \rightarrow H_2O_2 \quad (6)$$

$$\bullet OH + H_2O_2 \rightarrow HO_2^\bullet + H_2O \quad (7)$$

$$HO_2^\bullet + HO_2^\bullet \rightarrow H_2O_2 + O_2 \quad (8)$$

$$\bullet OH + HO_2^\bullet \rightarrow H_2O + O_2 \quad (9)$$
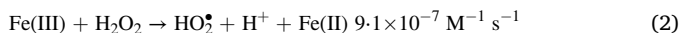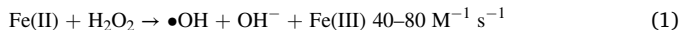
MXene are two-dimensional nitrides and carbides of transition metals and usually synthesized by stripping $M_{n+1}AX_n$ materials. Because of the individual two-dimensional layered structure, hydrophilicity, high metal conductivity, photothermal properties as well as large electrochemically active surfaces [21,22], a variety of MXene materials have been applied in energy storage, electromagnetic interference shielding, composite strengthening, gas/biosensors, lubrication as well as chemical catalysis [23–25]. The hydrogen fluoride etching route is commonly used for preparing the MXene materials [26]. For the past few years, due to the strong corrosive and toxic properties of hydrogen fluoride, a new type of nano-layered MAX phase and MXene batteries have been prepared by Lewis acid alkali molten salt leaching method [27–29]. Lewis acid is the late transition metal halides during their molten state, and strong electric bodies that are produced in these molten salts receive ligands that react thermodynamic with the A-site elements in the MAX phase (e.g., Si and Al) [30]. This means that the A-site elements of the classical MAX phase were replaced by transition metal halides. In the meantime, some forms of atoms or ions are able to be diffused into the two-dimensional plane to combine with non-saturable $M_{n+1}X_n$ thin slices and shape the matching MAX phase or MXene. The etching of lewis acid in molten salts affords an environmentally friendly and feasible way for the preparation of MXene without hydrogen fluoride. By reason that the presence of surface groups (e.g., -Cl, -O and -OH), MXene has strong hydrophilicity and electronegativity [31,32], it is expected to serve as an electron regulator or electron donor to boost the Fe(II) regeneration in the Fenton reaction. Nb_2C MXene consists of a carbon layer and two niobium layers [33], with thin atomic structure and rich in Nb, C and O elements, which may provide sufficient active sites for facilitating Fe (II)/Fe(III) redox couples. Therefore, Nb_2C MXene derived from Nb_2AlC MAX phase as the precursor was used as the co-catalyst to enhance Fenton oxidation for water decontamination.

In this study, Nb_2C MXene was synthesized by Lewis acid alkali melt salt stripping method [34], and applied to promote Fenton oxidation to degrade dimethyl phthalate (DMP). To our delight, Nb_2C MXene can strongly boost Fenton and Fenton-like reactions to activate peroxides (e. g., H_2O_2, PMS, PDS, and PAA) and generate reactive oxygen species (ROS). The $Nb_2C/Fe(III)/H_2O_2$ system can non-selectively degrade of various refractory pollutants with high stability during cyclic runs. By analyzing ROS, surface chemistry, iron species transformation and electrochemical properties, the deep mechanism of the $Nb_2C/Fe(III)/H_2O_2$ system was thoroughly investigated, focusing on the electron migration among Nb_2C MXene, iron species, and H_2O_2. Moreover, the routes of DMP degradation were analyzed based on the results of LC-QTOF-MS and Fukui index (DFT calculation). Therefore, this study proposed a novel scheme to boost Fenton oxidation by coupling 2D MXene and Fenton system, which exhibits high potential to realize environmental-friendly and continuable Fenton oxidation for eliminating refractory contaminants in water.

2. Materials and methods

2.1. Chemicals and materials

ANPEL Laboratory Technologies Inc afforded acetonitrile and methanol at HPLC grade. Iron(III) nitrate (Fe(III)), peroxymonosulfate (PMS), peroxydisulfate (PDS), peracetic acid (PAA), ferrous sulfate heptahydrate (Fe(II)), ethanol (ET), hydrogen peroxide (H_2O_2, 30 wt%), dimethyl phthalate (DMP), phenol (PE), diethyl phthalate (DEP), salicylic acid (2-HBA), 3-hydroxybenzoic acid (3-HBA), 4-hydroxybenzoic acid (4-HBA), 3,4-dihydroxybenzoic acid (3,4-HBA), benzoic acid (BA), acid orange 7 (AO7), bisphenol A (BPA), norfloxacin (NOR), ibuprofen (IBP), sulfamethoxazole (SMX), rhodamine B (RhB), 5,5-dimethyl-1-pyrolin-N-oxide (DMPO), coumarin, 7-hydroxycoumarin, *tert*-butyl alcohol (TBA), methyl phenyl sulfoxide (PMSO), isopropanol (IPA), sulfuric acid, sodium chloride, sodium sulfate, sodium nitrate, sodium bicarbonate, and nafion were purchased from Aladdin Industrial Corporation. The precursor of Nb_2AlC MXene (Nb_2AlC MAX) was obtained from Beike Nanomaterials Technology Co., Ltd. Materials include graphene (G), carbon nanotubes (CNT), diamond (ND), molybdenum (Mo), molybdenum disulfide (MoS_2), tungsten carbide (WC), and tungsten disulfide (WS_2) were from Aladdin Industrial Corporation, and prepared reduced graphene oxide (rGO) by calcination (Text S1).

2.2. Synthesis of niobium carbide materials

Niobium carbide (Nb_2C) MXene was prepared by alternative etching of Al layer elements of Nb_2AlC using a Lewis acid alkali molten salt stripping method (Scheme S1) [21,27,35]. 1.0 g Nb_2AlC, 3.0 g AgCl, 0.52 g NaCl, and 0.66 g KCl were mixed and milled for 20 min with the stoichiometric mole ratio of 1: 5: 2: 2. The mixtures were shifted to a railboat placed in the tubular furnace and roasted for 6 h, 12 h and 24 h at 700 °C in an argon atmosphere. The annealed Nb_2C MXene materials were first washed with ethanol, then further washed with ultra-pure water, and then dried by a vacuum freeze drier, which were finally labeled as Nb_2C-6, Nb_2C-12, and Nb_2C-24, respectively. In addition to Nb_2C, eight materials (Ti_2C-6, Ti_3C_2-6, Ti_3CN-6, Ta_2C-6, Ti_2C-12, Ti_3C_2-12, Ti_3CN-12 and Ta_2C-12) were prepared by Lewis acid alkali molten salt etching method for 6 h and 12 h, respectively [27].

2.3. Experiment procedure for degrading organic contaminants

The experiments of organic contaminants oxidation were performed in a beaker with 100 mL ultra-pure water and continuously stirred at a constant temperature (25 °C) (Text S2). The organic pollutants and iron species (Fe(II) or Fe(III) with desired dosage) were added into reaction solution, the solution pH was then controlled at 3.2 by 0.1 M ~ 1.0 M sulfuric acid. The experiments were started by contemporaneously adding required dosages of peroxides (H_2O_2, PMS, PDS, or PAA), co-catalyst (e.g., Nb_2C MXene, nanocarbons, or metal sulfides), and iron species (Fe(II) or Fe(III)). The 7 sampling times were set in 1 h, and the samples were filtered with 0.22 μm polyether sulfone membrane. The HPLC (Shimadzu 16) and the UV–vis spectrophotometer (UNICO UV2355) were employed to detect the concentrations of organic pollutants (Text S3). The concentration of diverse iron species and the concentration of H_2O_2 under different conditions were determined by spectrophotometric methods (Text S4 and Text 5). Intermediates from degradation of DMP were detected by a HPLC-quadrupole time of flight-mass spectrometer (LC-QTOF-MS, Agilent G6545) (Text S6). The Fukui functions of DMP and its degradation intermediates were calculated by Multiwfn (wave function analysis program) using Gaussian 16 software to analyze the degradation products and pathways of DMP [36]. TOC values in solution before and after reaction were measured by total
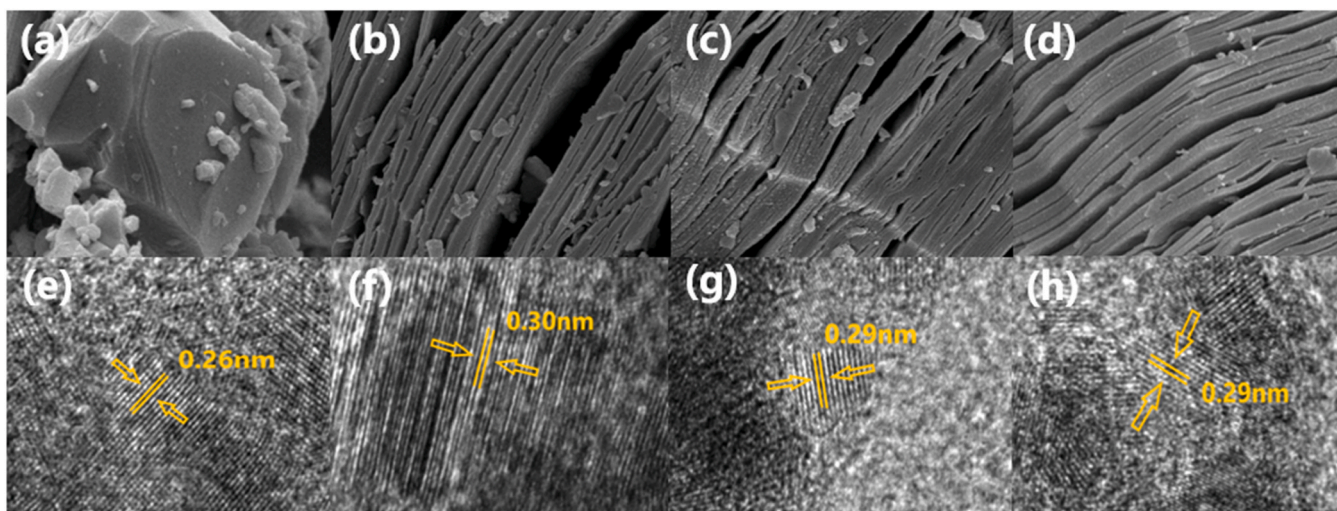
Fig. 1. SEM pictures of (a) Nb_2AlC, (b) Nb_2C-6, (c) Nb_2C-12, and (d) Nb_2C-24; HRTEM images of (e) Nb_2AlC, (f) Nb_2C-6, (g) Nb_2C-12, and (h) Nb_2C-24.

organic carbon analyzer (TOC-L CPH).

2.4. Analysis of ROS

For purpose of qualitatively analyzing the role of ROS for degrading DMP, the electron paramagnetic resonance (EPR) analysis was performed (Text S7). The contribution of •OH for DMP oxidation was investigated using TBA as the quenching agent. Moreover, coumarin and BA were selected as chemical probes for semi-quantitatively analyzing the concentrations of hydroxylation products induced by •OH [37]. In addition, PMSO was added into the experimental system to detect $PMSO_2$, the characteristic product derived from Fe(IV) induced

oxidation of PMSO via oxygen transfer, for analyzing the generation of Fe(IV). [38]. UHPLC methods were used to detect the concentrations of hydroxylation products of BA and coumarin, PMSO and $PMSO_2$ (Text S3).

2.5. Characterizations

The morphology of Nb_2C MXene at different calcination times was observed and compared by SEM (JSM-7500 F). The lattice spacing of Nb_2C MXene was analyzed by HRTEM (Talos F200S G2). The XPS (Thermo Fisher ESCALAB 250Xi), and FT-IR (PerkinElmer Spectrum Two), and Raman spectrometer (HORIBA LabRAM HR) were also used
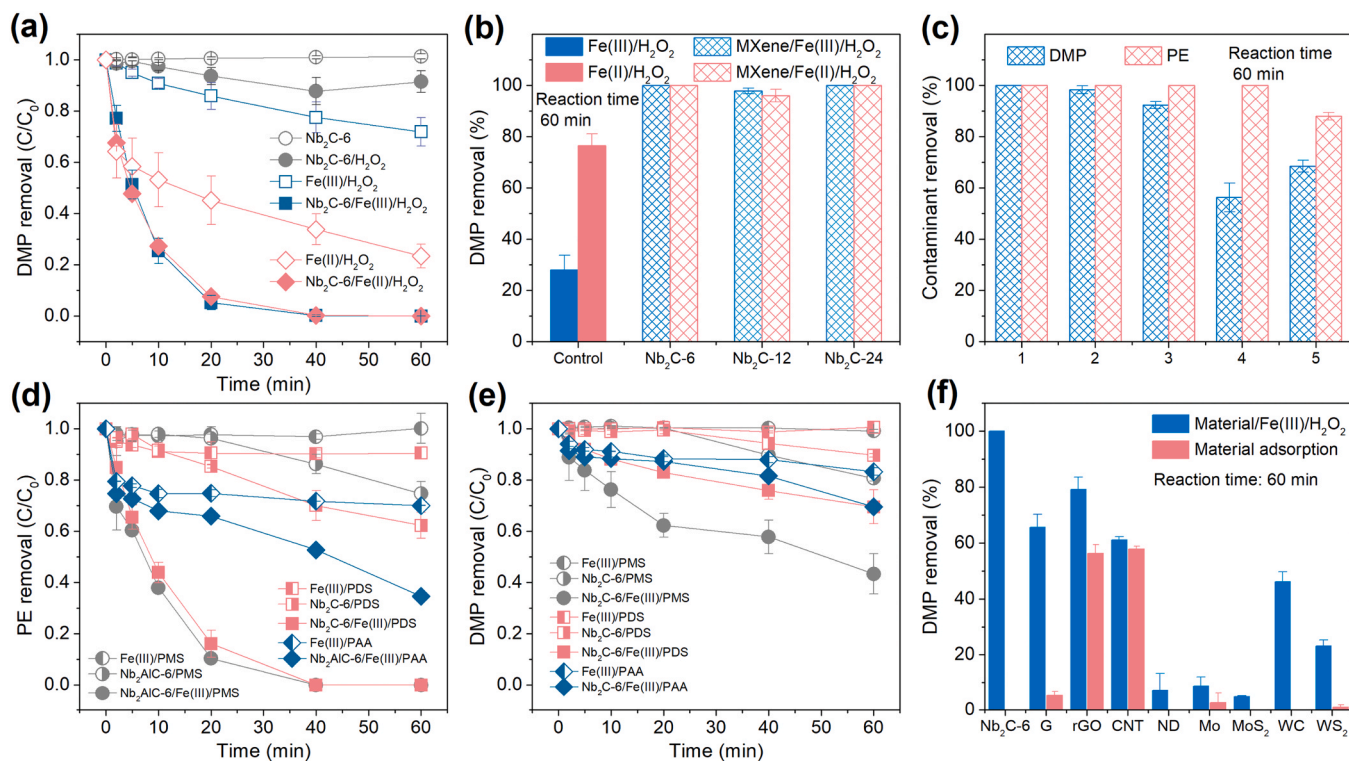

Fig. 2. DMP removal in (a) Nb_2C-6 and (b) Nb_2C-*x* boosted Fenton system; (c) cycling tests of Nb_2C-6 in the Nb_2C-6/Fe(III)/H_2O_2 system; (d) PE and (e) DMP removal in Nb_2C-6 boosted Fenton-like activation of peroxides; (f) comparison of Nb_2C-6 with other co-catalysts of Fenton system. Initial pH 3.2, peroxides (H_2O_2, PMS, PDS or PAA) 1.0 mM, Nb_2C-*x* 200 mg/L, Fe(III) or Fe(II) 20 μM, DMP or PE 20 μM.

to investigate the surface chemistry of Nb$_2$C MXene before and after reaction.
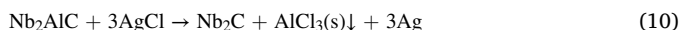
2.6. Electrochemical analysis

The redox capacity of iron species on Nb$_2$C MXene surface was investigated by electrochemical measurements on an electrochemical station (CHI 604E, China). 50 mL electrolyte solution with pH 3.2 was prepared with 0.2 mM Fe(III) and 50 mM sodium nitrate. The Nb$_2$C MXene coated glassy carbon electrode was prepared by mixing 10 g/L Nb$_2$C MXene, 2 mL isopropyl alcohol and 20 μL nafion perfluorinated resin in the sampling tube for 12 h, and then soaking in the electrode for natural air drying until the liquid evaporated. Nb$_2$C MXene coated glass carbon (working electrode), saturated calomel (reference electrode), and platinum wire (counter electrode) were selected for the electrochemical tests. In order to observe and compare the effects of Nb$_2$C MXene with different calcination times on iron redox capacity, OCP tests were performed and CV scans were recorded at a scanning rate of 0.05 V·s^{-1}.

3. Results and discussion

3.1. Characterization of Nb$_2$C MXene

Nb$_2$C MXene was made by Lewis acid alkali molten salt stripping method [30]. SEM image in Fig. 1a shows the blocky structure of original Nb$_2$AlC. The Nb$_2$AlC powders were immersed in the AgCl melt at 700 °C, the exposed Al atoms as the interlayer between Nb$_2$C layers are weakly bound to Nb and oxidized to Al(III) cations by Lewis acid Ag(I), forming solid AlCl$_3$ and accompanied by the reduction of Ag(I) to Ag^0 (Eq. 10), while Cl$^-$ reacts with Nb$_2$C to form Nb$_2$CCl to ensure charge compensation (Eq. 11) [27]. The prepared Nb$_2$CCl and Ag^0 mixture was soaked in ammonium persulfate solution to wipe off the Ag particles on the surface of Nb$_2$CCl MXene (Cl is the surface terminal), and also generate the base surface groups (including −OH and −Cl). Figs. 1b-1d show the SEM pictures of final etched specimens. After etching in molten salt, Nb$_2$AlC particles transform into accordion-like microstructure [33,39,40], which is similar to MXenes obtained by previously reported HF etching method [41]. The etching mechanism is no longer based on dangerous HF solutions, but a greener synthetic approach. The materials finally prepared by this molten salt etching route are named MS-Nb$_2$CT$_x$ MXene (MS denotes molten salt and T$_x$ denotes O and Cl surface groups) which are simply named Nb$_2$C MXene. In addition, HRTEM analysis shows that it is similar to MXene prepared by alkali assisted hydrothermal method [42,43], the interlayer spacings of Nb$_2$C-6 (0.30 nm, Fig. 1f), Nb$_2$C-12 (0.29 nm, Fig. 1g), and Nb$_2$C-24 (0.29 nm, Fig. 1h) are similar, which ware larger than that of the original Nb$_2$AlC (0.26 nm, Fig. 1e). Moreover, Nb$_2$C MXene synthesized by Lewis acid-alkali fused salt method has abundant surface groups (XPS spectra in Fig. S5, S12 and FT-IR spectra in Fig. S6, S13), which also means that it has a large number of surface sites, which lays a great foundation for the subsequent use as a co-catalyst of Fenton system [27,44].

$$Nb_2AlC + 3AgCl \rightarrow Nb_2C + AlCl_3(s)\downarrow + 3Ag \qquad (10)$$

$$Nb_2C + AgCl \rightarrow Nb_2CCl + Ag \qquad (11)$$

3.2. Performance of Nb$_2$C MXene for boosting Fenton oxidation

The reactivities of Nb$_2$C MXene for boosting Fenton and Fenton-like systems were evaluated towards the removal of DMP. Fig. 2a depicts that Nb$_2$C-6 MXene cannot effectively adsorb DMP (< 2.0%) and also cannot directly activate H$_2$O$_2$ to remove DMP (< 10%). The Fe(III)/H$_2$O$_2$ system can only degrade 28% DMP at 60 min, illustrating the low reactivity of Fe(III) for inducing Fenton chain reaction to produce ROS.

However, the coupling of Nb$_2$C-6 with Fe(III)/H$_2$O$_2$ can completely remove DMP within 40 min, which proves the high performance of Nb$_2$C-6 to enhance Fenton oxidation. For the traditional Fenton system (Fe(II)/H$_2$O$_2$), the degradation curve of DMP can be divided into the rapid stage (k_{obs} = 0.054 min^{-1}) and the pursuant slow stage (k_{obs} = 0.016 min^{-1}) (Fig. S1). The oxidation capacity of Fenton (Fe(II)/H$_2$O$_2$) system can also be strongly raised by Nb$_2$C MXene. During whole reaction progress, the efficient degradation of DMP in the Nb$_2$C-6/Fe(II)/H$_2$O$_2$ system is well in accord with the pseudo-first order kinetic model (k_{obs} = 0.15 min^{-1}). Although Nb$_2$C-6, Nb$_2$C-12 and Nb$_2$C-24 were synthesized with different calcination times, Fig. 2b and Fig. S2 demonstrate that all of these Nb$_2$C MXene can achieve almost 100% DMP removal within 60 min by coupling with Fe(III)/H$_2$O$_2$ or Fe(II)/H$_2$O$_2$. Moreover, a wide variety of MXene materials (Ti$_2$C-6, Ti$_3$C$_2$-6, Ti$_3$CN-6, Ta$_2$C-6, Ti$_2$C-12, Ti$_3$C$_2$-12, Ti$_3$CN-12 and Ta$_2$C-12) exhibit the capabilities to boost Fenton oxidation for degrading DMP (Fig. S3 and S4), implying that it is may be the widespread property of MXene materials for boosting Fenton oxidation. Due to the highest reactivity to enhance Fenton oxidation for DMP removal, Nb$_2$C-6 was selected as the typical MXene material for further mechanism investigation.

Moreover, the reusability of Nb$_2$C-6 for boosting the Fe(III)/H$_2$O$_2$ system was analyzed with five successive cycling tests towards the oxidation of DMP and PE. The Nb$_2$C-6/Fe(III)/H$_2$O$_2$ system shows high capability for long-term oxidation of organic contaminants, high removal efficiencies of DMP (69%) and PE (88%) were also obtained at fifth run (Fig. 2c). XPS, FTIR, and Raman results show that the surface functional groups and the structural defects (I_D/I_G) of Nb$_2$C-6 changed slightly after 5 cyclic tests, indicating the high stability of Nb$_2$C-6 for long-term operation in the Nb$_2$C-6/Fe(III)/H$_2$O$_2$ system (Fig. S5~S7). Nb$_2$C MXene also exhibit high reactivity for Fenton-like reactions to promote iron-mediated peroxide O-O bonds decomposition of all kinds of peroxides to generate ROS [45,46]. Fig. 2d and Fig. 2e depict the degradation of PE and DMP in Nb$_2$C-6 co-catalyzed Fenton-like activation of various peroxides, respectively. 100% PE removal were obtained in systems of Nb$_2$C-6/Fe(III)/H$_2$O$_2$, Nb$_2$C-6/Fe(III)/PMS, and Nb$_2$C-6/Fe(III)/PDS, and the Nb$_2$C-6/Fe(III)/PAA system can also degrade 65% PE removal, indicating that Nb$_2$C can strengthen the Fenton-like reaction to activate a variety of peroxides for producing ROS. In the systems of Nb$_2$C-6 boosted Fenton-like activation of PMS, PDS and PAA, the removal ratio of DMP were 57%, 31% and 30%, respectively, which was markedly lower than that of the Nb$_2$C-6/Fe(III)/H$_2$O$_2$ system (100%). The kinetic analysis shows that apparent rate constant (k_{obs}) of DMP removal in the Nb$_2$C-6/Fe(III)/H$_2$O$_2$ system is significantly higher than that of other three peroxides (PMS, PDS, and PAA) assisted systems (0.140 min^{-1} (H$_2$O$_2$) > 0.013 min^{-1} (PMS) > 0.006 min^{-1} (PDS) > 0.005 min^{-1} (PAA), Fig. S8), indicating that ●OH produced in the Nb$_2$C-6/Fe(III)/H$_2$O$_2$ system is more preponderant for degrading DMP in Nb$_2$C mediated Fenton and Fenton-like systems due to the non-selective oxidation feature of ●OH.

The inputs of diversiform co-catalysts are an effective strategy for boosting Fenton and Fenton-like oxidation, such as metal sulfides [17,47,48], zero valent metals [48], metal carbides and carbon materials [47]. For further evaluating the reactivity of Nb$_2$C, the performance of Nb$_2$C-6 was then compared with a variety of co-catalysts assisted Fe(III)/H$_2$O$_2$ systems. It well documented that metal-free carbon materials can significantly accelerate the rate-limiting process of chain reactions in Fenton systems by directly donating electrons for Fe(III) reduction or mediating electron transport from H$_2$O$_2$ to Fe(III) [49–51]. Fig. 2f indicates that by coupling with G, rGO, CNT, and ND at 60 min, the DMP removal efficiency was increased from 28% (Fe(III)/H$_2$O$_2$) to 66%, 79%, 61%, and 7%, respectively. The Fe(II) regeneration can also be accelerated by introducing transition metal-based electron-rich materials as electron sacrifices [52,53], however, MoS$_2$, WS$_2$, Mo, and WC assisted Fe(III)/H$_2$O$_2$ systems attain relatively low DMP removal ratios at 60 min. Nevertheless, the Nb$_2$C-6/Fe(III)/H$_2$O$_2$ system can completely degrade DMP at 60 min, these results indicate that Nb$_2$C-6 well outperforms than

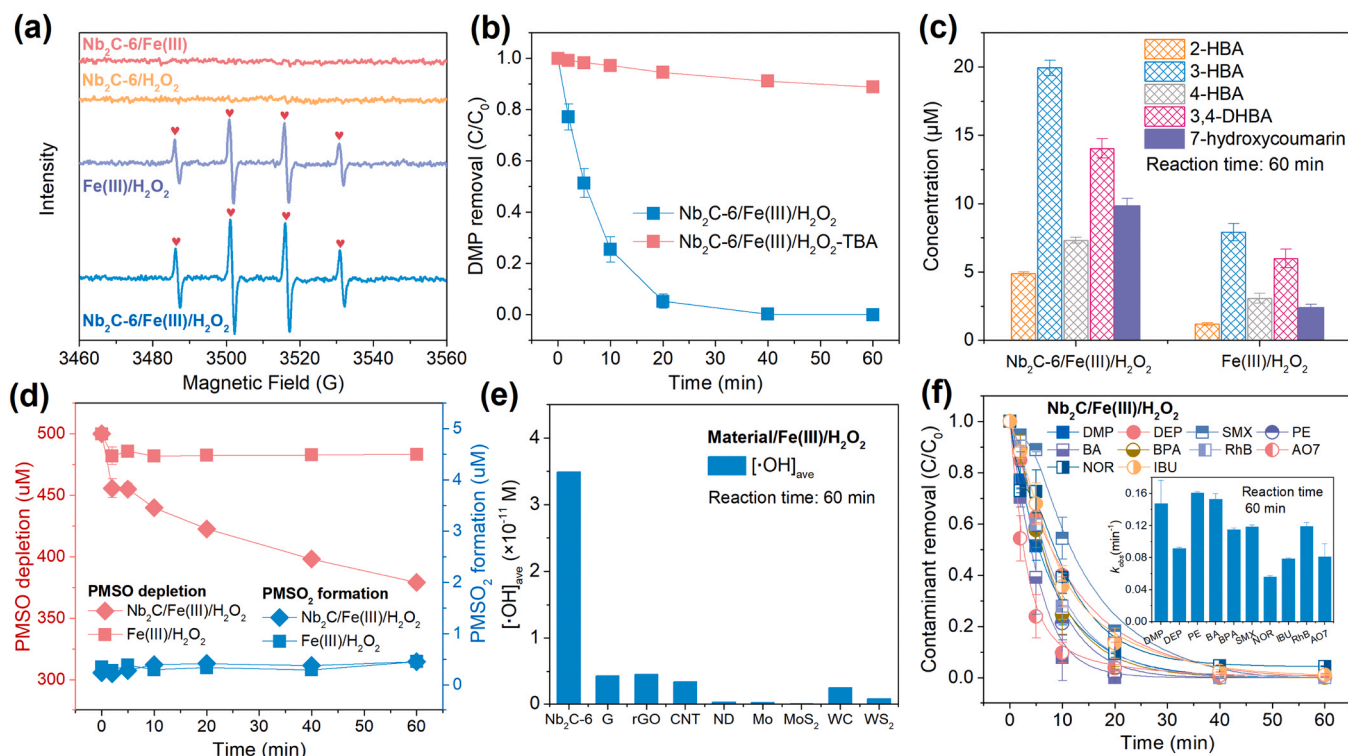**Fig. 3.** (a) EPR spectra, (b) quenching tests, (c) chemical probe experiments using BA and coumarin (for ●OH), (d) chemical probe tests using PMSO (for Fe(IV)), (e) the steady-state concentration of ●OH ([●OH]$_{ave}$) in various co-catalysts assisted Fe(III)/H$_2$O$_2$ systems, (f) removal of multifarious pollutants in the Nb$_2$C-6/Fe(III)/H$_2$O$_2$ system. Initial pH 3.2, H$_2$O$_2$ 1 mM, Fe(III) 20 μM, (a) Nb$_2$C-6 200 mg/L, DMPO 20 mM; (b) Nb$_2$C-6 200 mg/L, DMP 20 μM, TBA 20 mM; (c) Nb$_2$C-6 200 mg/L, BA 0.2 mM or coumarin 0.5 mM; (d) Nb$_2$C-6 200 mg/L, PMSO 0.5 mM; (e) co-catalyst 200 mg/L, DMP 20 μM; (f) Nb$_2$C-6 200 mg/L, contaminants 20 μM.

all of these reported co-catalysts for boosting Fenton systems.

3.3. Identification of ROS

The significantly accelerated H$_2$O$_2$ consumption in the Nb$_2$C-6/Fe(III)/H$_2$O$_2$ system compared with non-material system indicates that Nb$_2$C-6 may promote the decomposition of H$_2$O$_2$ to generate ROS by boosting Fenton chain reactions (Fig. S9). Hydroxyl radicals are generally considered to be the main ROS in the classical Fenton reaction, while DMPO acts as an *in situ* spin trapping agent for conducting EPR test to analyze the formation of ROS in the Nb$_2$C-6/Fe(III)/H$_2$O$_2$ system. As can be seen from Fig. 3a, there was no distinct peaks of specific adduct appear in spectra obtained from the systems of Nb$_2$C-6/Fe(III) and Nb$_2$C-6/H$_2$O$_2$. However, in systems of Fe(III)/H$_2$O$_2$ and Nb$_2$C-6/Fe(III)/H$_2$O$_2$, the features of DMPO-OH adducts were detected with the specific quartet peaks (1:2:2:1) and the splitting constants ($\alpha^N = \alpha^H = 14.9$ g), implying the generation of ●OH [54]. The intension of DMPO-OH adduct in the Nb$_2$C-6/Fe(III)/H$_2$O$_2$ system is markedly stronger than that in the system without material, indicating that Nb$_2$C-6 can significantly accelerate Fenton reaction to generate ●OH. Additionally, the contribution of ●OH for DMP removal was investigated by adding TBA as the ●OH scavenger [55]. As shown in Fig. 3b, DMP was completely degraded at 60 min without adding TBA. Whereas, when the addition of TBA was 20 mM, the DMP degradation rate was lower than 10% at 60 min, which significantly inhibited the removal of DMP. Thus, the quenching test reveals that ●OH is the major ROS for degrading DMP in the Nb$_2$C-6/Fe(III)/H$_2$O$_2$ system.

For further semi-quantitative analysis of ●OH, chemical probe tests using BA and coumarin were carried out by detecting their specific hydroxylation products [56]. Fig. 3c depicts that the Nb$_2$C-6/Fe(III)/H$_2$O$_2$ system can produce 4.9 μM 2-HBA, 20.0 μM 3-HBA, 7.3 μM 4-HBA, 14.0 μM 3,4-DHBA with the addition of 0.2 mM BA, respectively, which are markedly higher than these in the Fe(III)/H$_2$O$_2$ system.

Moreover, when coumarin was used as the chemical probe, the output of 7-hydroxycoumarin amplified from 2.4 μM (control group) to 9.9 μM. The significantly growth of outputs of BA and coumarin products in the Nb$_2$C-6/Fe(III)/H$_2$O$_2$ system manifests that Nb$_2$C-6 affords for promoting the formation of ●OH.

In the classic Fenton system, ●OH is the primary ROS for oxidizing organic compounds under acidic conditions. In the Nb$_2$C-6/Fe(III)/H$_2$O$_2$ system, the generation of Fe(IV) needs to be further identified to analyze the leading role of ●OH for the oxidation of organic contaminants. It has been reported that sulfoxides are oxidized by Fe(IV) to form corresponding sulfoxides through the oxygen atom transfer approach markedly different from ●OH induced products [57]. Consequently, PMSO was often used as a chemical probe to determine whether Fe(IV) is formed [38]. Fig. 3d depicts the Nb$_2$C-6/Fe(III)/H$_2$O$_2$ system can significantly degrade PMSO (120.7 μM), however, only 0.46 μM PMSO$_2$ was generated at 60 min. The conversion rate from PMSO to PMSO$_2$ is extremely low (0.4%), implying that the contribution of Fe(IV) for contaminant oxidation in the Nb$_2$C-6/Fe(III)/H$_2$O$_2$ system can be neglected. Therefore, tests by employing EPR, quenching and chemical probes verified that hydroxyl radicals are the major ROS produced in the Nb$_2$C/Fe(III)/H$_2$O$_2$ system.

In addition, the steady-state concentration of ●OH ([●OH]$_{ave}$) of the Nb$_2$C-6/Fe(III)/H$_2$O$_2$ system was calculated using a kinetic model by comparing with 9 co-catalysts assisted Fe(III)/H$_2$O$_2$ systems (Text S8, Fig. S10 and S11) [3]. Fig. 3e illustrates that [●OH]$_{ave}$ in the Nb$_2$C-6/Fe(III)/H$_2$O$_2$ system is 3.49×10^{-11} M, which is 8 ~ 106 folds than these in nanocarbons (G (0.43×10^{-11} M), rGO (0.46×10^{-11} M), CNT (0.35×10^{-11} M), ND (0.33×10^{-12} M)), zero valent metal (Mo (0.28×10^{-12} M)), metal sulfides (WS$_2$ (0.83×10^{-12} M), MoS$_2$ (0.10×10^{-12} M)), and metal carbide (WC (0.25×10^{-11} M)) boosted Fe(III)/H$_2$O$_2$ systems [50,52,53]. Kinetic analysis further reveals that Nb$_2$C-6 can significantly promote Fenton reaction to generate ●OH, the reactivity of Nb$_2$C is extremely higher than previously reported co-catalysts.
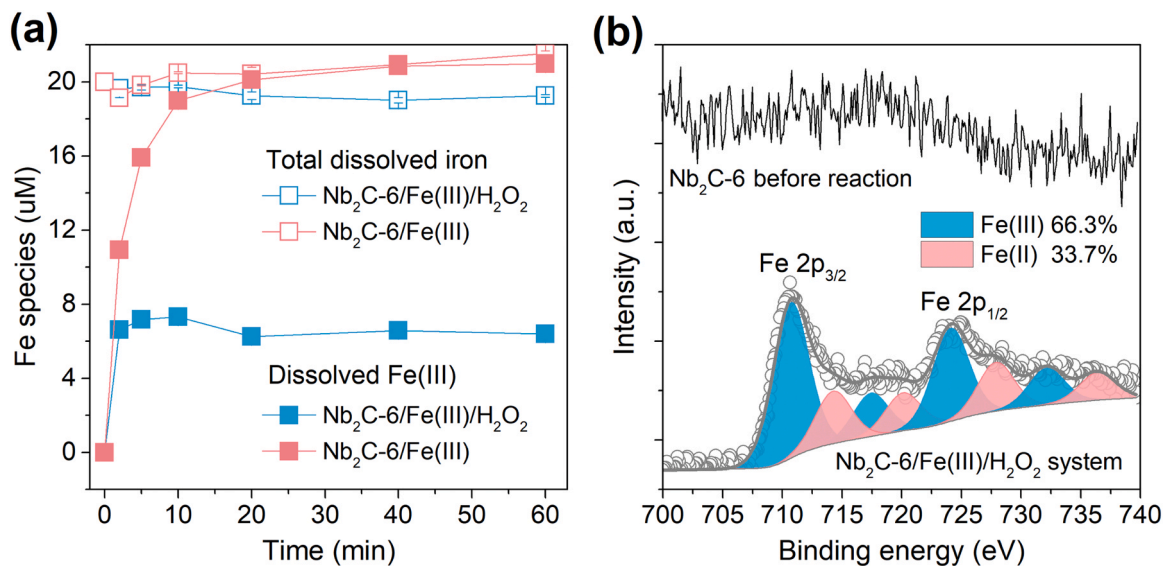
Fig. 4. (a) Conversion of iron species in the Nb_2C-6 mediated systems, (b) Fe 2p XPS spectra of original and residual Nb_2C-6. Initial pH 3.2, DMP 20 μM, H_2O_2 1.0 mM, Nb_2C-6 200 mg/L, Fe(III) 20 μM.
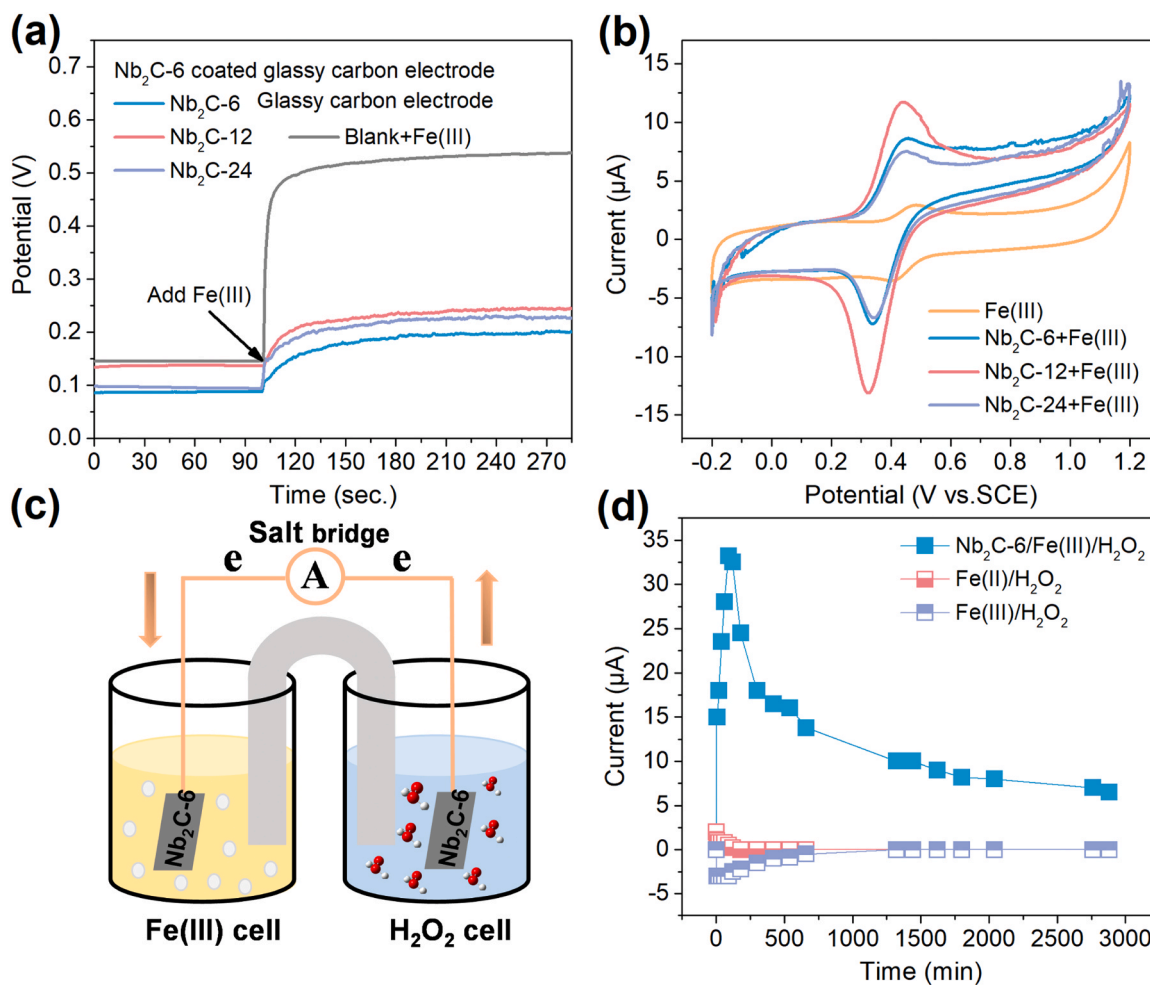

Fig. 5. (a) OCP curves of Fe(III) species on Nb_2C-6/Nb_2C-12/Nb_2C-24 surface, (b) CV scans of pristine and Nb_2C-6/Nb_2C-12/Nb_2C-24 coated glassy carbon electrodes, Initial pH 3.2, Fe(III) 200 μM, Nb_2C-6 10 g/L, $NaNO_3$ 50 mM; (c) GOP reaction device setup, (d) current variation between Fe(III)/Fe(II) and H_2O_2 in Fenton-like system coated with Nb_2C-6. Initial pH 3.2, DMP 20 μM, H_2O_2 1 mM, Nb_2C-6 10 g/L, Fe(III) 20 μM.
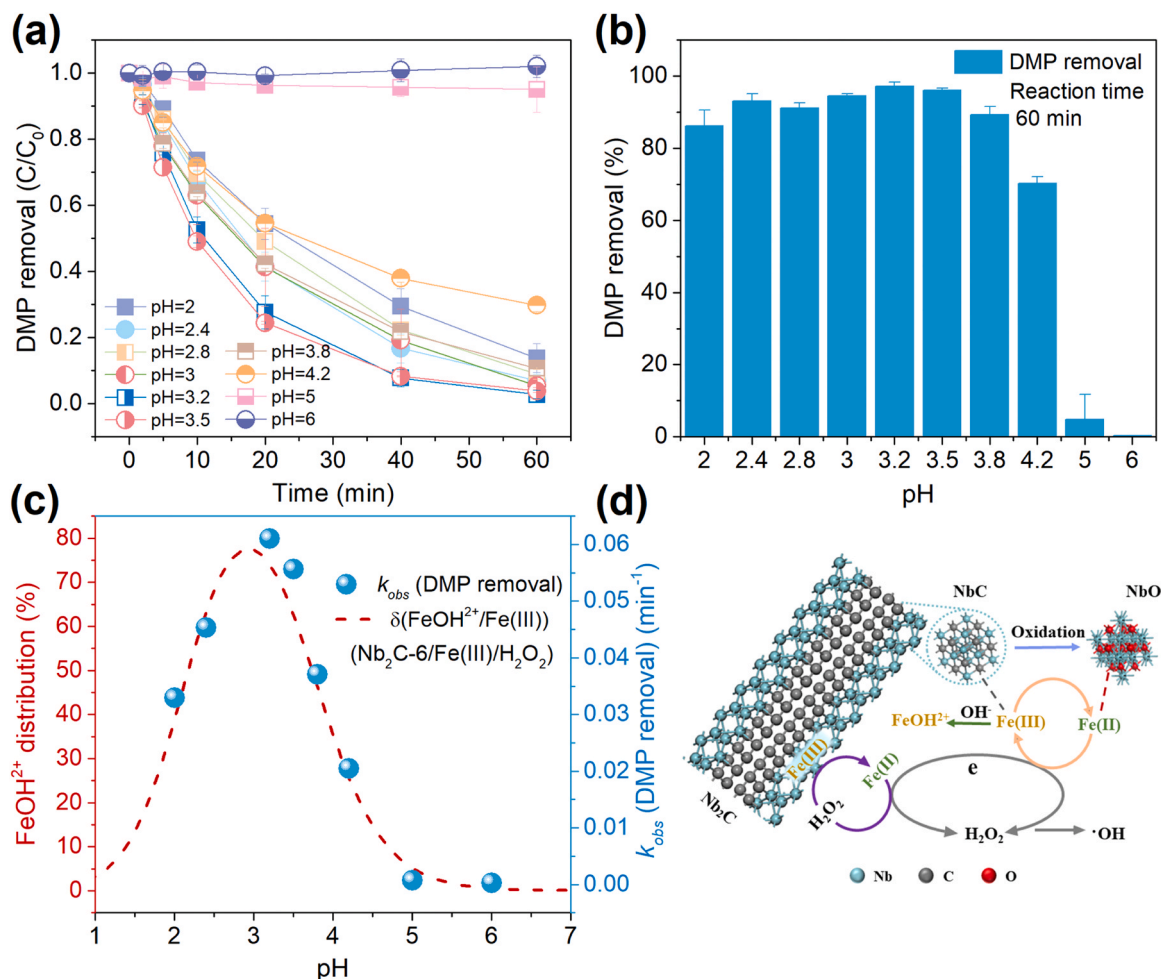
Fig. 6. (a) Removal curve and (b) removal ratio of DMP in the Nb$_2$C-6/Fe(III)/H$_2$O$_2$ system at pH ranging from 2.0 to 6.0, (c) comparison of k_{obs} and distribution fraction of Fe(III) at pH ranging from 1.0 to 7.0, (d) mechanism of the Nb$_2$C-6/Fe(III)/H$_2$O$_2$ system. Initial pH 2.0 ~ 6.0, DMP 20 μM, H$_2$O$_2$ 1 mM, Nb$_2$C-6 200 mg/L, Fe(III) 20 μM.

Resulting from the production of •OH in high concentration, the Nb$_2$C-6/Fe(III)/H$_2$O$_2$ system can non-selectively and thoroughly oxidize various organic pollutants with diverse molecular structures, such as PAEs (DMP and DEP), dyes (RhB and AO7), phenols (PE and BPA), drugs (SMX, NOR, and IBU) as well as other aromatic compound (BA) (Fig. 3f). Therefore, Nb$_2$C MXene is expected to act as a green and efficient co-catalyst to enhance Fenton oxidation and further degrade a broad spectrum of organic pollutants for environmental remediation.

3.4. Mechanism investigation

3.4.1. Nb$_2$C accelerated Fe(III) reduction

The rate-limiting step for producing ROS by Fenton chain reactions is Fe(III) reduction [49]. Therefore, the conversion of iron species was detected to unveil the mechanism of Nb$_2$C-6 enhanced Fenton chemistry. Fig. 4a illustrates that Fe(III) was almost completely converted into Fe(II) within 10 min in the Nb$_2$C-6/Fe(III) system, revealing Fe(III) can be straightly and rapidly reduced by Nb$_2$C-6. According to high-resolution XPS spectra in Fig. 4b, the original Nb$_2$C-6 is an iron-free material. However, after reaction from the Nb$_2$C-6/Fe(III)/H$_2$O$_2$ system, a pair of Fe(II) peaks (714 eV and 727 eV) presented in the Fe 2p spectrum of Nb$_2$C-6 with 66.3% Fe(III) and 33.7% Fe(II). This indicates that the transformation of Fe species occurs on Nb$_2$C-6 surface. Fig. 4a also depicts that most of iron species in the Nb$_2$C-6/Fe(III)/H$_2$O$_2$ system existed in dissolved forms. Although Fe(III) reduction occurs on Nb$_2$C surface, the *in-situ* generated Fe(II) can further decompose H$_2$O$_2$ for
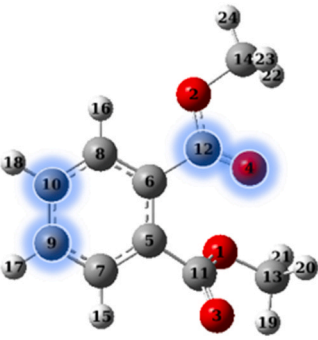
producing •OH primarily via homogeneous Fenton reaction, rather than Nb$_2$C-iron complexes catalyzed heterogeneous Fenton reaction.

The above results proved that Fe(III) can be directly reduced by Nb$_2$C-6, indicating the potential functional groups act as active sites on Nb$_2$C-6 surface for electron donation. XPS spectra of C1s and Nb 3d (Fig. S5 and S12) and FTIR spectra (Fig. S6 and S13) indicate that the existence of various functional groups on the surface of Nb$_2$C-6. High-resolution XPS spectra of Nb 3d and C 1 s exhibit that the Nb-C peaks corresponding at 203.8 eV and 281.3 eV and the C=O peak corresponding at 531.1 eV decreased significantly after the reaction [58]. The FTIR spectra show that there was no obvious peak of C=C before the reaction, but appeared a marked C=C peak (1630 cm^{-1}) after three cyclic tests. It is inferred that some new functional groups are constantly formed on the surface of Nb$_2$C-6 during reaction in the Nb$_2$C-6/Fe (III)/H$_2$O$_2$ system. According to the analysis of XPS and FTIR, it can be inferred that the fracture of Nb-C bond on the surface of Nb$_2$C-6 can provide electrons for Fe(III) reduction and further accelerate Fe(II) catalyzed H$_2$O$_2$ decomposition to produce •OH, while NbC was oxidized to NbO.

The effect of the dosages of Nb$_2$C-6, Fe(III) and H$_2$O$_2$ on DMP removal in the Nb$_2$C-6/Fe(III)/H$_2$O$_2$ system were tested (Fig. S14), and the apparent kinetic constants were calculated by fitting the kinetic model (Fig. S15 and Table S1~S3). According to the apparent kinetic of Eq. 12~14 [17], it is able to be found that the absolute value of the reaction order of [Fe(III)] (1.36) is much larger than that of [Nb$_2$C-6] (0.62) and [H$_2$O$_2$] (0.26). The effect of Nb$_2$C-6 was weak, indicating that

Table 1
Fukui index of DMP and natural population analysis.

Chemical structure of DMP	Atom	q (N)	q (N + 1)	q (N-1)	f	f^+	f^0	CDD
	1(O)	-0.128	-0.142	-0.088	0.040	0.015	0.027	-0.026
	2(O)	-0.123	-0.157	-0.096	0.027	0.034	0.031	0.007
	3(O)	-0.268	-0.335	-0.118	0.150	0.067	0.108	-0.083
	4(O)	-0.262	-0.348	-0.192	0.070	0.086	0.078	0.017
	5(C)	0.003	-0.063	0.080	0.077	0.066	0.071	-0.012
	6(C)	-0.009	-0.078	0.039	0.048	0.069	0.059	0.022
	7(C)	-0.026	-0.067	0.021	0.047	0.041	0.044	-0.006
	8(C)	-0.030	-0.078	0.017	0.047	0.048	0.048	0.001
Dimethyl phthalate	**9(C)**	-0.027	-0.122	0.033	0.060	0.095	0.077	0.035
Dimethyl phthalate	**10(C)**	-0.032	-0.107	0.073	0.105	0.075	0.090	-0.030
	11(C)	0.208	0.174	0.242	0.034	0.034	0.034	0.000
	12(C)	0.206	0.134	0.224	0.018	0.072	0.045	0.054
	13(C)	0.009	-0.008	0.026	0.018	0.016	0.017	-0.001
	14(C)	0.009	-0.011	0.024	0.015	0.020	0.018	0.005
	15(H)	0.053	0.021	0.083	0.030	0.032	0.031	0.001
	16(H)	0.046	0.015	0.078	0.032	0.031	0.032	-0.001
	17(H)	0.051	0.003	0.088	0.037	0.048	0.042	0.011
	18(H)	0.050	0.007	0.094	0.044	0.043	0.043	-0.001
	19(H)	0.042	0.024	0.060	0.018	0.018	0.018	0.000
	20(H)	0.047	0.034	0.062	0.015	0.012	0.014	-0.003
	21(H)	0.046	0.027	0.069	0.023	0.019	0.021	-0.005
	22(H)	0.045	0.027	0.057	0.013	0.017	0.015	0.005
	23(H)	0.045	0.026	0.058	0.014	0.019	0.016	0.005
	24(H)	0.047	0.024	0.066	0.019	0.023	0.021	0.004

Nb_2C-6 could provide a mass of active sites on its surface, and a small amount of Nb_2C-6 could achieve a better degradation effect. The Fe(III) dosage has a prominent effect on DMP removal, and the effect of Fe(III) dosage on DMP removal is much greater than these of Nb_2C-6 dosage or H_2O_2 dosage, indicating that iron species mediated route is the main way to activate H_2O_2 and generate •OH via Fenton reaction. To our delight, the amount of Nb dissolved in the solution after reaction was detected, and the Nb leaching in the Nb_2C-6/Fe(III)/H_2O_2 system is extremely low (< 30 µg/L, Fig. S16). It would not cause secondary pollution to environmental waters, thus Nb_2C-6 could be used as a green material.

$$-(dc/dt) = K \times [Nb_2C\text{-}6]^a \times [Fe(III)]^b \times [H_2O_2]^c \tag{12}$$

$$\log(-dc/dt) = \log K + a\log[Nb_2C\text{-}6] + b\log[Fe(III)] + c\log[H_2O_2] \tag{13}$$

$$\log(-dc/dt) = K[Nb_2C\text{-}6]^{0.62}[Fe(III)]^{1.36}[H_2O_2]^{0.26} \tag{14}$$

*3.4.2. Nb_2C mediated electron transfer between H_2O_2 and iron species*

Morphological monitoring of iron species and XPS analysis show that the low capacity of adsorption and chelation of Nb_2C-6 towards Fe(III) and Fe(II). Whereas, according to XPS spectra of Nb_2C-6 before and after reaction, the surface of Nb_2C-6 may also have a weak combination capability with Fe(III) for improving the Fe(III) reactivity (Fig. 4a). The electrochemical experiments (OCP and CV) were carried out for comparing the reactivity of Fe(III) on Nb_2C-x surface. The OCP values of Fe(III) on GCE after coating Nb_2C-6, Nb_2C-12, and Nb_2C-24 decrease to 0.26 V, 0.28 V, and 0.26 V, respectively, compared with that of Fe(III) on GCE without material coating (0.54 V) (Fig. 5a). Compared with nitrogen-doped carbon nanotubes which possesses the ability to increase the oxidation potential of Fe(III) (Fig. S17), the addition of Nb_2C decreased the OCP values of Fe(III). According to the previous experimental results in Fig. 4a, the decrease of the value of oxidation potential in OCP tests is due to Nb_2C induced Fe(III) reduction. In addition, in Fig. 5b CV curves, peak redox currents appeared during the analysis of Nb_2C-6, Nb_2C-12, and Nb_2C-24, indicating that Nb_2C can be used as an excellent mediator in Fenton system for expediting Fe(III)/Fe(II) cycle. The current enhancement reveals the conversion of Fe(II)/Fe(III) can be significantly accelerated.

For exploring the principle of electron transfer between iron species

and H_2O_2 in the Nb_2C-6/Fe(III)/H_2O_2 system, salt bridge experiments were performed (Fig. 5c). The current between electrodes during reaction process and the concentrations of iron species and H_2O_2 before and after reaction were monitored. The orientation of electron transfer was estimated by analyzing the the direction of current during the reaction process, so as to investigate the reaction mechanism. The peak value increased to 33.2 µA at 1.5 h, then decreased to 6.5 µA at 48 h in the Nb_2C-6/Fe(III)/H_2O_2 system (Fig. 5d). Moreover, the weak current (< 4.0 µA) was tested in the Fe(III)/H_2O_2 system, while the current in the Fe(II)/H_2O_2 system is negligible. It was observed that the current flowed from one side of Fe(III) to the other side of H_2O_2 in the Fe(III)/H_2O_2 system, manifesting that electrons were transferred from H_2O_2 to Fe(III) for the further generation of Fe(II). At the beginning and end of the experiment, iron species and H_2O_2 concentration were tested. During the reaction, Fe(II) was generated (3.54 µM) and H_2O_2 was decomposed (0.29 mM), which is consistent with the results of electron transfer between iron species and H_2O_2 mediated by Nb_2C-6 MXene. However, the detected current was extremely feeble (< 4.0 µA) in the Fe(III)/H_2O_2 system (Table S4). After coating materials, the direction of current is opposite in the Nb_2C/Fe(III)/H_2O_2 system, which is identical to that in the Fe(II)/H_2O_2 system, indicating that electrons shift from Fe(II) to H_2O_2 via Nb_2C MXene. At the end of the test, 10.27 µM of Fe(III) was converted into Fe(II) and 0.46 mM H_2O_2 was decomposed in the Nb_2C/Fe(III)/H_2O_2 system. Because Fe(II) reacts quickly with H_2O_2, a large current (33.2 µA) is detected in this process. In addition, there was almost no current detected in the Fe(II)/H_2O_2 system. The salt bridge test shows that the direct reduction of Fe(III) occurs with Nb_2C-6 as the electron donor, and Nb_2C-6 can further mediate the electron transfer between Fe(II) and H_2O_2 to expedite •OH generation for environmental remediation.

3.5. pH-dependent property of Nb_2C boosted Fenton oxidation

In Fenton system, Fe(III)/Fe(II) circularly catalyzed chain reactions can generate •OH to degrade organic contaminants, solution pH is crucial for Fenton oxidation resulting from the pH-dependent variation of iron species. Figs. 6a-6b indicate that the Nb_2C-6/Fe(III)/H_2O_2 system is sensitive to solution pH, and the high removal ratio of DMP achieved at the pH range of 2.0 to 4.2. The optimal degradation efficiency reaches 100% at pH 3.2, however, the removal ratio of DMP is extremely low (< 5%) at pH > 5.0. In general, Fe(III) primarily exists as Fe^{3+}, $FeOH^{2+}$,
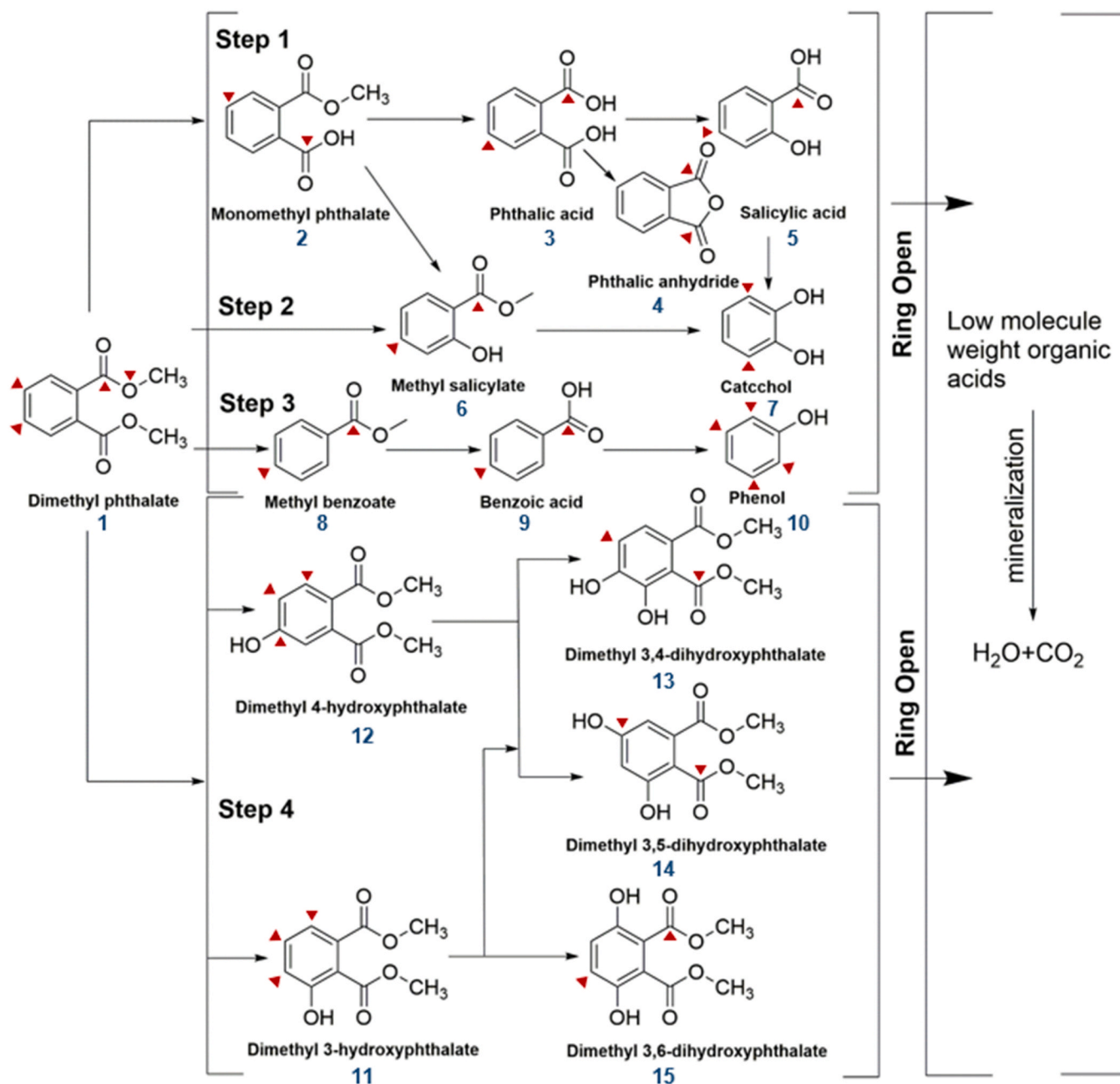
Scheme 1. DMP degradation route in the Nb_2C-6/Fe(III)/H_2O_2 system.

and $Fe(OH)_2^+$ at the high efficiency pH window of 2.0 ~ 4.2 (Fig. S18a), while Fe(II) basically lives in the form of Fe^{2+} (Fig. S18b). The oxidation capacity of the Nb_2C-6/Fe(III)/H_2O_2 system is remarkably affected by the form of Fe(III) species. Afterwards, the distributions of iron species and the k_{obs} of DMP removal were further compared. Results show that the major Fe(III) species is $FeOH^{2+}$ when pH was 3.2 (Fig. S18), it is more easily reduced to Fe^{2+} by H_2O_2 and Nb_2C-6. In addition, the well-fitting curve between the distribution coefficient of $FeOH^{2+}$ and k_{obs} of DMP removal in Fig. 6c further confirms that the leading active Fe(III) species responsible for triggering Fenton chain reactions and generate •OH is $FeOH^{2+}$.

Hence, Nb_2C-6 as an electron donor can directly reduce Fe(III) with the transformation from NbC to NbO on its surface in the Nb_2C-6/Fe (III)/H_2O_2 system. Meanwhile, Nb_2C-6 can also mediate electron transfer from Fe(II) to H_2O_2 to promote the generation of •OH in the Nb_2C-6/Fe(III)/H_2O_2 system. Moreover, the O-O bond length of H_2O_2

(1.471 Å) is longer than other three peroxides (PMS 1.326 Å, PDS 1.222 Å, and PAA 1.443 Å), and it is easier to participate in the reaction [59]. H_2O_2 thus outperformed than other three peroxides for Nb_2C boosted Fenton and Fenton-like systems (Figs. 2d and 2e). $FeOH^{2+}$ is identified as the main active Fe(III) species to accelerate the oxidation-reduction cycle of Fe(III)/Fe(II), resulting in promotion of •OH formation in Fenton chain reactions (Fig. 6d).

3.6. Degradation pathways of DMP

DMP is a common short-chain ester with a high solubility and a long half-life in water, so it is not easily degraded in water and has potential toxic hazards to biological environment and human health. For the past few years, the effective removal of DMP in aquatic environment has caused wide consideration [60]. For analyzing DMP degradation routes in the Nb_2C/Fe(III)/H_2O_2 system, the main intermediates derived from

DMP oxidation were tested by UHPLC-QTOF-MS technology. In this system, eleven different types of aromatic intermediates were detected (Table S5, Fig. S19~S27), including methyl phthalate, salicylic acid, phthalic acid, phthalic anhydride, methyl salicylic acid, methyl benzoate, catechol, phenol, benzoic acid, dimethyl-3-hydroxyphthalate, and dimethyl-2,4-dihydroxyphthalate divalent acid ester. On this basis, the Fukui functions of DMP and its intermediate products were calculated based on DFT calculation, and the Hirschfeld charges of each element of each substance in N, N + 1 and N-1 electronic forms are calculated by the concentrated Fukui function (Table S6~S20). According to the corresponding Fukui functions, the occurrence of electrophilic attack or nucleophilic attack can be speculated on each site. The degradation of DMP is mainly attacked by •OH, and •OH induced nucleophilic reaction will gradually degrade to produce low molecular weight substances. For f^+ of DMP, the four largest values at O4, C9, C10 and C12 are the sites most prone to nucleophilic attack (Table 1). In the same way, the active sites of other intermediates were analyzed and the degradation routes were put forward as Scheme 1.

As shown in Scheme 1, in the initial stage, DMP was hydrolyzed or eliminated and further oxidized to form methyl benzoate [60], accompanied by the production of methyl salicylate. These aromatic esters will be further degraded to produce aromatic acids and phenolic substances (e.g., phthalic acid, benzoic acid, catechol and phenol). In another pathway, DMP can be oxidized to dimethyl-3-hydroxyl phthalate, which will be further oxidized to dimethyl-2,4-dihydroxyl phthalate. Therefore, DMP degradation mainly produces aromatic esters through four routes: 1) extraction of methoxyl to form mono-methyl phthalate; 2) extraction of methyl formate to form methyl salicylate; 3) removal of methyl formate to form methyl benzoate; 4) hydroxylation to form more complex esters. These intermediates can be further decomposed into organic acids with low molecular weights. The $Nb_2C-6/Fe(III)/H_2O_2$ system can achieve 37.3% TOC removal after 4 h reaction (Fig. S28). Combining with the detection of 11 types of intermediates derived from DMP, the $Nb_2C-6/Fe(III)/H_2O_2$ system can degrade and further mineralized DMP by producing •OH.

4. Conclusions

The sluggish conversion from Fe(III) to Fe(II) in Fenton/Fenton-like systems strongly limits the persistent generation of hydroxyl radicals in Fenton system for long-term removal of refractory contaminants. In this study, the oxidation capacity of the $Fe(III)/H_2O_2$ system were significantly enhanced by Nb_2C-6 by promoting the formation of •OH. Meanwhile, the oxidation performance of Nb_2C-6 in Fenton/Fenton system is better than that of nanocarbons, zero valent metal, metal sulfides, and metal carbide. The technical merits of Nb_2C-6 boosted Fenton oxidation include non-selective oxidation capability, strong stability for long-term operation as well as less secondary pollution. The mechanism investigation proves that Nb_2C-6 can provide electrons for Fe(III) reduction by cleaving Nb-C bonds meanwhile mediate the electron transport between Fe(II) and H_2O_2, resulting in acceleration of •OH formation and DMP degradation. In addition, the degradation pathways of DMP were proposed based on the results of UHPLC-QTOF-MS tests and Fukui function. This study puts forward a novel strategy for the application of two-dimensional MXene materials in enhanced Fenton/Fenton-like oxidation, MXene materials are promising as efficient co-catalysts to surmount the limitation of Fenton reaction and promote Fenton chemistry towards the green and long-lasting future.

CRediT authorship contribution statement

Zixuan Zhang: Conceptualization, Methodology, Investigation, Data curation, Materials synthesis, Writing – original draft, Writing – review & editing. **Chenying Zhou:** Investigation, Methodology. **Yiming Sun:**

Materials synthesis. **Peng Zhou:** Conceptualization, Methodology, Supervision, Validation, Resources, Project administration, Funding acquisition, Writing - review & editing. **Yang Liu:** Conceptualization supervision, Methodology. **Heng Zhang:** Methodology. **Ye Du:** Methodology. **Chuanshu He:** Conceptualization supervision, Investigation, Methodology. **Zhaokun Xiong:** Conceptualization, Supervision, Project administration. **Bo Lai:** Conceptualization, Supervision, Project administration, Funding acquisition, Writing – review & editing.

Declaration of Competing Interest

The authors declare that they have no known competing financial interests or personal relationships that could have appeared to influence the work reported in this paper.

Data Availability

Data will be made available on request.

Acknowledgements

Appendix A. Supporting information

Supplementary data associated with this article can be found in the online version at doi:10.1016/j.apcatb.2023.123385.

References

[1] J. Zhang, C. Zhang, Y. Zhu, J. Li, X. Li, Biodegradation of seven phthalate esters by Bacillus mojavensis B1811, Int. Biodeterior. Biodegrad. 132 (2018) 200–207, https://doi.org/10.1016/j.ibiod.2018.04.006.

[2] Y. Zhang, Y. Jiao, Z. Li, Y. Tao, Y. Yang, Hazards of phthalates (PAEs) exposure: A review of aquatic animal toxicology studies, Sci. Total Environ. 771 (2021), 145418, https://doi.org/10.1016/j.scitotenv.2021.145418.

[3] W. Ren, P. Zhou, G. Nie, C. Cheng, X. Duan, H. Zhang, S. Wang, Hydroxyl radical dominated elimination of plasticizers by peroxymonosulfate on metal-free boron: Kinetics and mechanisms, Water Res 186 (2020), 116361, https://doi.org/10.1016/j.watres.2020.116361.

[4] C.J. Salim, H. Liu, J.F. Kennedy, Comparative study of the adsorption on chitosan beads of phthalate esters and their degradation products, Carbohydr. Polym. 81 (3) (2010) 640–644, https://doi.org/10.1016/j.carbpol.2010.03.024.

[5] P. Zhou, J. Zhang, Z. Xiong, Y. Liu, X. Huo, X. Cheng, W. Li, F. Cheng, Y. Zhang, C_{60} Fullerol promoted $Fe(III)/H_2O_2$ Fenton oxidation: Role of photosensitive Fe(III)-Fullerol complex, Appl. Catal. B 265 (2020), 118264, https://doi.org/10.1016/j.apcatb.2019.118264.

[6] Y. Jiang, J. Ran, K. Mao, X. Yang, L. Zhong, C. Yang, X. Feng, H. Zhang, Recent progress in Fenton/Fenton-like reactions for the removal of antibiotics in aqueous environments, Ecotoxicol. Environ. Saf. 236 (2022), 113464, https://doi.org/10.1016/j.ecoenv.2022.113464.

[7] Y. Zhu, R. Zhu, Y. Xi, J. Zhu, G. Zhu, H. He, Strategies for enhancing the heterogeneous Fenton catalytic reactivity: A review, Appl. Catal. B 255 (2019), 117739, https://doi.org/10.1016/j.apcatb.2019.05.041.

[8] S. Ziembowicz, M. Kida, Limitations and future directions of application of the Fenton-like process in micropollutants degradation in water and wastewater treatment: A critical review, Chemosphere 296 (2022), 134041, https://doi.org/10.1016/j.chemosphere.2022.134041.

[9] Z. Yang, A. Yu, C. Shan, G. Gao, B. Pan, Enhanced Fe(III)-mediated Fenton oxidation of atrazine in the presence of functionalized multi-walled carbon nanotubes, Water Res 137 (2018) 37–46, https://doi.org/10.1016/j.watres.2018.03.006.

[10] H. Dihingia, D. Tiwari, Impact and implications of nanocatalyst in the Fenton-like processes for remediation of aquatic environment contaminated with micro-pollutants: A critical review, J. Water Process. Eng. 45 (2022), 102500, https://doi.org/10.1016/j.jwpe.2021.102500.

[11] Y. Zhang, M. Zhou, A critical review of the application of chelating agents to enable Fenton and Fenton-like reactions at high pH values, J. Hazard. Mater. 362 (2019) 436–450, https://doi.org/10.1016/j.jhazmat.2018.09.035.

[12] B. Song, Z. Zeng, E. Almatrafi, M. Shen, W. Xiong, C. Zhou, W. Wang, G. Zeng, J. Gong, Pyrite-mediated advanced oxidation processes: Applications, mechanisms,

and enhancing strategies, Water Res 211 (2022), 118048, https://doi.org/10.1016/j.watres.2022.118048.

[13] B. Anusha, M. Anbuchezhiyan, R. Sribalan, N. Srinivasan, alias Arunsankar, Synergistic effect of TiO₂-rGO nanocomposites with Fenton's reagent for the enhanced photocatalytic degradation of nitrophenols in solar light, Appl. Phys. A. 128 (5) (2022) 411, https://doi.org/10.1007/s00339-022-05554-5.

[14] Y. Ding, W. Huang, Z. Ding, G. Nie, H. Tang, Dramatically enhanced Fenton oxidation of carbamazepine with easily recyclable microscaled CuFeO₂ by hydroxylamine: Kinetic and mechanism study, Sep. Purif. Technol. 168 (2016) 223–231, https://doi.org/10.1016/j.seppur.2016.05.043.

[15] M.J. Zhao, L. Jung, Kinetics of the competitive degradation of deoxyribose and other molecules by hydroxyl radicals produced by the Fenton reaction in the presence of ascorbic acid, Free Radic. Res. 23 (3) (1995) 229–243, https://doi.org/10.3109/10715769509064036.

[16] F.S.Yaxin Qin, Zhihui Ai, Pingping Zhang, Lizhi Zhang, Protocatechuic Acid Promoted Alachlor Degradation in Fe(III)/H₂O₂ Fenton System, Environ. Sci. Technol. 49 (13) (2015) 7948–7956, https://doi.org/10.1021/es506110w.

[17] M. Xing, W. Xu, C. Dong, Y. Bai, J. Zeng, Y. Zhou, J. Zhang, Y. Yin, Metal Sulfides as Excellent Co-catalysts for H₂O₂ Decomposition in Advanced Oxidation Processes, Chem 4 (6) (2018) 1359–1372, https://doi.org/10.1016/j.chempr.2018.03.002.

[18] Q. Yan, J. Zhang, M. Xing, Cocatalytic Fenton Reaction for Pollutant Control, Cell. Rep. Phys. Sci. 1 (8) (2020), 100149, https://doi.org/10.1016/j.xcrp.2020.100149.

[19] P. Zhou, W. Ren, G. Nie, X. Li, X. Duan, Y. Zhang, S. Wang, Fast and Long-Lasting Iron(III) Reduction by Boron Toward Green and Accelerated Fenton, Chem., Angew. Chem. Int. Ed. 59 (38) (2020) 16517–16526, https://doi.org/10.1002/anie.202007046.

[20] P. Zhou, Y. Yang, W. Ren, X. Li, Y. Zhang, B. Lai, S. Wang, X. Duan, Molecular and kinetic insights to boron boosted Fenton-like activation of peroxymonosulfate for water decontamination, Appl. Catal. B 319 (2022), 121916, https://doi.org/10.1016/j.apcatb.2022.121916.

[21] S. Tu, J. Li, X. Zhang, X. Liu, J. Tang, Effect of surfactants on the morphology of ferroelectric crystals grown from MXene, AIP Adv. 11 (11) (2021), 115121, https://doi.org/10.1063/5.0070118.

[22] Y. Zhang, L. Wang, N. Zhang, Z. Zhou, Adsorptive environmental applications of MXene nanomaterials: a review, RSC Adv. 8 (36) (2018) 19895–19905, https://doi.org/10.1039/c8ra03077d.

[23] B. Anasori, M.R. Lukatskaya, Y. Gogotsi, 2D metal carbides and nitrides (MXenes) for energy storage, Nat. Rev. Mater. 2 (2) (2017) 16098, https://doi.org/10.1038/natrevmats.2016.98.

[24] T. Kshetri, D.T. Tran, H.T. Le, D.C. Nguyen, H.V. Hoa, N.H. Kim, J.H. Lee, Recent advances in MXene-based nanocomposites for electrochemical energy storage applications, Prog. Mater. Sci. 117 (2021), 100733, https://doi.org/10.1016/j.pmatsci.2020.100733.

[25] A. VahidMohammadi, J. Rosen, Y. Gogotsi, The world of two-dimensional carbides and nitrides (MXenes), 1165-+, Science 372 (6547) (2021) https://doi.org/10.1126/science.abf1581.

[26] M. Anayee, N. Kurra, M. Alhabeb, M. Seredych, M.N. Hedhili, A.H. Emwas, H. N. Alshareef, B. Anasori, Y. Gogotsi, Role of acid mixtures etching on the surface chemistry and sodium ion storage in Ti₃C₂Tₓ MXene, Chem. Commun. 56 (45) (2020) 6090–6093, https://doi.org/10.1039/d0cc01042a.

[27] Y. Li, H. Shao, Z. Lin, J. Lu, L. Liu, B. Duployer, P.O.A. Persson, P. Eklund, L. Hultman, M. Li, K. Chen, X.H. Zha, S. Du, P. Rozier, Z. Chai, E. Raymundo-Pinero, P.L. Taberna, P. Simon, Q. Huang, A general Lewis acidic etching route for preparing MXenes with enhanced electrochemical performance in non-aqueous electrolyte, Nat. Mater. 19 (8) (2020) 894–899, https://doi.org/10.1038/s41563-020-0657-0.

[28] J. Xu, T. Peng, X. Qin, Q. Zhang, T. Liu, W. Dai, B. Chen, H. Yu, S. Shi, Recent advances in 2D MXenes: preparation, intercalation and applications in flexible devices, J. Mater. Chem. A 9 (25) (2021) 14147–14171, https://doi.org/10.1039/d1ta03070a.

[29] H. Dong, P. Xiao, N. Jin, B. Wang, Y. Liu, Z. Lin, Molten Salt Derived Nb₂CTₓ MXene Anode for Li-ion Batteries, ChemElectroChem 8 (5) (2021) 957–962, https://doi.org/10.1002/celc.202100142.

[30] M. Li, J. Lu, K. Luo, Y. Li, K. Chang, K. Chen, J. Zhou, J. Rosen, L. Hultman, P. Eklund, P.O.A. Persson, S. Du, Z. Chai, Z. Huang, Q. Huang, Element Replacement Approach by Reaction with Lewis Acidic Molten Salts to Synthesize Nanolaminated MAX Phases and MXenes, J. Am. Chem. Soc. 141 (11) (2019) 4730–4737, https://doi.org/10.1021/jacs.9b00574.

[31] V.M. Hong Ng, H. Huang, K. Zhou, P.S. Lee, W. Que, J.Z. Xu, L.B. Kong, Recent progress in layered transition metal carbides and/or nitrides (MXenes) and their composites: synthesis and applications, J. Mater. Chem. A 5 (7) (2017) 3039–3068, https://doi.org/10.1039/c6ta06772g.

[32] S. Zhang, W.Q. Han, Recent advances in MXenes and their composites in lithium/sodium batteries from the viewpoints of components and interlayer engineering, Phys. Chem. Chem. Phys. 22 (29) (2020) 16482–16526, https://doi.org/10.1039/d0cp02275f.

[33] W. Zhou, B. Yu, J. Zhu, K. Li, S. Tian, Hierarchical ZnO/MXene (Nb₂C and V₂C) heterostructure with efficient electron transfer for enhanced photocatalytic activity, Appl. Surf. Sci. 590 (2022), 153095, https://doi.org/10.1016/j.apsusc.2022.153095.

[34] Y. Bai, C. Liu, T. Chen, W. Li, S. Zheng, Y. Pi, Y. Luo, H. Pang, MXene-Copper/Cobalt Hybrids via Lewis Acidic Molten Salts Etching for High Performance Symmetric Supercapacitors, Angew. Chem. Int. Ed. 60 (48) (2021) 25318–25322, https://doi.org/10.1002/anie.202112381.

[35] M. Naguib, J. Halim, J. Lu, K.M. Cook, L. Hultman, Y. Gogotsi, M.W. Barsoum, New two-dimensional niobium and vanadium carbides as promising materials for Li-ion batteries, J. Am. Chem. Soc. 135 (43) (2013) 15966–15969, https://doi.org/10.1021/ja405735d.

[36] T. Lu, F. Chen, Multiwfn: a multifunctional wavefunction analyzer, J Comput Chem. 33(5), 580–592, https://doi.org/10.1002/jcc.22885.

[37] T. Zhang, Y. Wen, Z. Pan, Y. Kuwahara, K. Mori, H. Yamashita, Y. Zhao, X. Qian, Overcoming Acidic H₂O₂/Fe(II/III) Redox-Induced Low H₂O₂ Utilization Efficiency by Carbon Quantum Dots Fenton-like Catalysis, Environ. Sci. Technol. 56 (4) (2022) 2617–2625, https://doi.org/10.1021/acs.est.1c06276.

[38] X. Li, J. Ma, Y. Gao, X. Liu, Y. Wei, Z. Liang, Enhanced atrazine degradation in the Fe(III)/peroxymonosulfate system via accelerating Fe(II) regeneration by benzoquinone, Chem. Eng. J. 427 (2022), 131995, https://doi.org/10.1016/j.cej.2021.131995.

[39] D. Zu, H. Song, Y. Wang, Z. Chao, Z. Li, G. Wang, Y. Shen, C. Li, J. Ma, One-pot in-situ hydrothermal synthesis of CdS/Nb₂O₅/Nb₂C heterojunction for enhanced visible-light-driven photodegradation, Appl. Catal. B 277 (2020), 119140, https://doi.org/10.1016/j.apcatb.2020.119140.

[40] C. Song, W. Zhang, Q. Jin, Y. Zhang, X. Wang, Z. Bakenov, In-situ constructed accordion-like Nb₂C/Nb₂O₅ heterostructure as efficient catalyzer towards high-performance lithium-sulfur batteries, J. Power Sources 520 (2022), 230902, https://doi.org/10.1016/j.jpowsour.2021.230902.

[41] M. Alhabeb, K. Maleski, B. Anasori, P. Lelyukh, L. Clark, S. Sin, Y. Gogotsi, Guidelines for Synthesis and Processing of Two-Dimensional Titanium Carbide (Ti₃C₂Tₓ MXene), Chem. Mater. 29 (18) (2017) 7633–7644, https://doi.org/10.1021/acs.chemmater.7b02847.

[42] T. Li, L. Yao, Q. Liu, J. Gu, R. Luo, J. Li, X. Yan, W. Wang, P. Liu, B. Chen, W. Zhang, W. Abbas, R. Naz, D. Zhang, Fluorine-Free Synthesis of High-Purity Ti₃C₂Tₓ (T=OH, O) via Alkali Treatment, Angew. Chem. Int. Ed. 57 (21) (2018) 6115–6119, https://doi.org/10.1002/anie.201800887.

[43] W. Feng, H. Luo, Y. Wang, S. Zeng, Y. Tan, H. Zhang, S. Peng, Ultrasonic assisted etching and delaminating of Ti₃C₂ Mxene, Ceram. Int. 44 (6) (2018) 7084–7087, https://doi.org/10.1016/j.ceramint.2018.01.147.

[44] G. Li, S. Peng, B. He, J. Wang, Y. Du, W. Zhang, K. Han, F. Dang, Highly Efficient Nb₂C MXene Cathode Catalyst with Uniform O-Terminated Surface for Lithium-Oxygen Batteries, Adv. Energy Mater. 11 (1) (2020) 2002721, https://doi.org/10.1002/aenm.202002721.

[45] S. Wacławek, H.V. Lutze, K. Grübel, V.V.T. Padil, M. Černík, D.D. Dionysiou, Chemistry of persulfates in water and wastewater treatment: A review, Chem. Eng. J. 330 (2017) 44–62, https://doi.org/10.1016/j.cej.2017.07.132.

[46] M.F. He, W.Q. Li, Z.H. Xie, S.R. Yang, C.S. He, Z.K. Xiong, Y. Du, Y. Liu, F. Jiang, Y. Mu, B. Lai, Peracetic acid activation by mechanochemically sulfidated zero valent iron for micropollutants degradation: Enhancement mechanism and strategy for extending applicability, Water Res 222 (2022), 118887, https://doi.org/10.1016/j.watres.2022.118887.

[47] S. Shao, G. Wang, Z. Gong, M. Wang, J. Hu, J. Peng, K. Lu, S. Gao, Insights into the role of hydroxyl group on carboxyl-modified MWCNTs in accelerating atenolol removal by Fe(III)/H₂O₂ system, Chem. Eng. J. 425 (2021), 130581, https://doi.org/10.1016/j.cej.2021.130581.

[48] A. Goswami, J.-Q. Jiang, M. Petri, Treatability of five micro-pollutants using modified Fenton reaction catalysed by zero-valent iron powder (Fe(0)), J. Environ. Chem. Eng. 9 (4) (2021), 105393, https://doi.org/10.1016/j.jece.2021.105393.

[49] C. Zhou, P. Zhou, M. Sun, Y. Liu, H. Zhang, Z. Xiong, J. Liang, S. Duan, B. Lai, Nitrogen-doped carbon nanotubes enhanced Fenton chemistry: Role of near-free iron(III) for sustainable iron(III)/iron(II) cycles, Water Res 210 (2022), 117984, https://doi.org/10.1016/j.watres.2021.117984.

[50] Y. Sun, P. Zhou, P. Zhang, S. Meng, C. Zhou, Y. Liu, H. Zhang, Z. Xiong, X. Duan, B. Lai, New insight into carbon materials enhanced Fenton oxidation: A strategy for green iron(III)/iron(II) cycles, Chem. Eng. J. 450 (2022) 138423, https://doi.org/10.1016/j.cej.2022.138423.

[51] F. Cheng, P. Zhou, Y. Liu, X. Huo, J. Zhang, Y. Yuan, H. Zhang, B. Lai, Y. Zhang, Graphene oxide mediated Fe(III) reduction for enhancing Fe(III)/H₂O₂ Fenton and photo-Fenton oxidation toward chloramphenicol degradation, Sci. Total Environ. 797 (2021), 149097, https://doi.org/10.1016/j.scitotenv.2021.149097.

[52] Y. Yang, Q. Wang, R. Aleisa, T. Zhao, S. Ma, G. Zhang, T. Yao, Y. Yin, MoS₂/FeS Nanocomposite Catalyst for Efficient Fenton Reaction, ACS Appl. Mater. Interfaces 13 (44) (2021) 51829–51838, https://doi.org/10.1021/acsami.1c02864.

[53] C. Dong, J. Ji, B. Shen, M. Xing, J. Zhang, Enhancement of H₂O₂ Decomposition by the Co-catalytic Effect of WS₂ on the Fenton Reaction for the Synchronous Reduction of Cr(VI) and Remediation of Phenol, Environ. Sci. Technol. 52 (19) (2018) 11297–11308, https://doi.org/10.1021/acs.est.8b02403.

[54] J.M. Fontmorin, R.C. Burgos Castillo, W.Z. Tang, M. Sillanpaa, Stability of 5,5-dimethyl-1-pyrroline-N-oxide as a spin-trap for quantification of hydroxyl radicals in processes based on Fenton reaction, Water Res 99 (2016) 24–32, https://doi.org/10.1016/j.watres.2016.04.053.

[55] C. Guo, X. Qin, R. Guo, Y. Lv, M. Li, Z. Wang, T. Li, Optimization of heterogeneous Fenton-like process with Cu-Fe@CTS as catalyst for degradation of organic matter in leachate concentrate and degradation mechanism research, Waste Manag. 134 (2021) 220–230, https://doi.org/10.1016/j.wasman.2021.08.021.

[56] Y. Cai, J. Fan, Z. Liu, Enhanced degradation of tetracycline over FeS-based Fenton-like process: autocatalytic decomposition of H₂O₂ and reduction of Fe(III), J. Hazard. Mater. 436 (2022), 129092, https://doi.org/10.1016/j.jhazmat.2022.129092.

[57] H. Bataineh, O. Pestovsky, A. Bakac, pH-induced mechanistic changeover from hydroxyl radicals to iron(iv) in the Fenton reaction, Chem. Sci. 3 (5) (2012) 1594–1599, https://doi.org/10.1039/c2sc20099f.

[58] M. Lian, Y. Shi, W. Zhang, J. Zhao, D. Chen, Nitrogen and sulfur co-doped Nb_2C-MXene nanosheets for the ultrasensitive electrochemical detection dopamine under acidic conditions in gastric juice, J. Electroanal. Chem. 904 (2022), 115849, https://doi.org/10.1016/j.jelechem.2021.115849.

[59] X. Duan, H. Sun, L. Zhou, G. Wang, S. Wang, Insights into N-doping in single-walled carbon nanotubes for enhanced activation of superoxides: a mechanistic study, Chem. Comm. 168 (2015), 115143, https://doi.org/10.1039/C5CC05101K.

[60] J. Xue, Z. Zhu, Y. Zong, C. Huang, M. Wang, Oxidative degradation of dimethyl phthalate (DMP) by the Fe(VI)/H_2O_2 process, ACS Omega 4 (5) (2019) 9467–9472, https://doi.org/10.1021/acsomega.9b01012.